Oxidative Strong Metal–Support Interactions between Metals and Inert Boron Nitride

Article *in* Journal of Physical Chemistry Letters · April 2021

DOI: 10.1021/acs.jpclett.1c00934

13 authors, including:

Jinhu Dong
Dalian Institute of Chemical Physics
14 PUBLICATIONS **286** CITATIONS
SEE PROFILE

Rongtan Li
Dalian Institute of Chemical Physics
10 PUBLICATIONS **213** CITATIONS
SEE PROFILE

Bing Yang
Chongqing Medical University
35 PUBLICATIONS **871** CITATIONS
SEE PROFILE

Bai Yunxing
Dalian Institue of Chemical Physics. Chinese Academy of Sciences
19 PUBLICATIONS **302** CITATIONS
SEE PROFILE

THE JOURNAL OF PHYSICAL CHEMISTRY LETTERS
A JOURNAL OF THE AMERICAN CHEMICAL SOCIETY

pubs.acs.org/JPCL

Letter

Oxidative Strong Metal–Support Interactions between Metals and Inert Boron Nitride

Tongyuan Song,[#] Jinhu Dong,[#] Rongtan Li, Xiaoyan Xu, Matsumoto Hiroaki, Bing Yang, Rankun Zhang, Yunxing Bai, Hui Xin, Le Lin, Rentao Mu, Qiang Fu,[*] and Xinhe Bao

Cite This: *J. Phys. Chem. Lett.* 2021, 12, 4187–4194

Read Online

ACCESS | Metrics & More | Article Recommendations | Supporting Information

ABSTRACT: The strong metal–support interaction (SMSI) is one of the most important concepts in heterogeneous catalysis, which has been widely investigated between metals and active oxides triggered by reductive atmospheres. Here, we report the oxidative strong metal–support interaction (O-SMSI) effect between Pt nanoparticles (NPs) and inert hexagonal boron nitride (h-BN) sheets, in which Pt NPs are encapsulated by oxidized boron (BO_x) overlayers derived from the h-BN support under oxidative conditions. De-encapsulation of Pt NPs has been achieved by washing in water, and the residual ultrathin BO_x overlayers work synergistically with surface Pt sites for enhancing CO oxidation reaction. The O-SMSI effect is also present in other h-BN-supported metal catalysts such as Au, Rh, Ru, and Ir within different oxidative atmospheres including O_2 and CO_2, which is determined by metal–boron interaction and O affinity of metals.

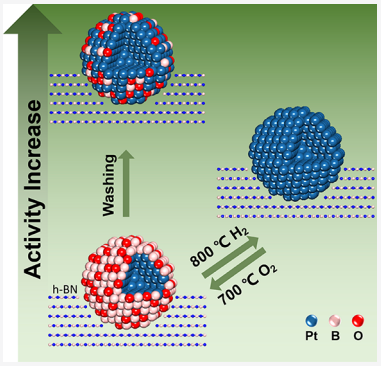

Hexagonal boron nitride (h-BN) has recently attracted wide attention in many heterogeneous catalytic reactions[1−6] due to its unique surface chemical and electronic properties.[7] It has been reported that h-BN shows excellent performance in oxidative dehydrogenation of ethane[8] and propane,[1,2] which is attributed to the active BO_x or B-OH species produced on the h-BN surface.[9−11] As catalyst supports, h-BN enriched with B/N vacancies or BO_x groups can form interfacial bonds with metals, which affects the morphology and electronic structure of the supported metals[12−17] and further tunes their catalytic performance. For instance, Cao et al.[18] found that Ni catalyst supported on h-BN nanosheets showed anti-coking and anti-sintering properties in dry reforming of methane (DRM) reaction. B and N vacancies modified the electronic structure of the Ni catalyst and facilitated the activation of CO_2. Liu et al.[19] found that Pt nanoparticles (NPs) preferred to be stabilized at the edges of h-BN nanosheets, which made them easier to be reduced under propane combustion conditions than those on basal planes of h-BN. Additionally, the classical strong metal–support interaction (SMSI) effect between Ni and h-BN has been demonstrated,[20] in which Ni NPs are encapsulated with permeable BO_x overlayers induced by DRM reaction, and the surface B-O/B-OH sites work synergistically with surface Ni sites to catalyze the reaction.

The classical SMSI effect has been extensively investigated in the catalysis and surface science communities[21−26] since it was discovered by Tauster et al. in 1978.[27] Triggered by high-temperature reduction, metal catalysts in the SMSI state feature prominently in the encapsulation by support-derived material, which has been widely observed in transition metal oxides (TiO_2, Fe_3O_4, CeO_2, etc.)-supported group VIII metals.[28−30] Until now, very few studies have reported the classical SMSI effect in oxidizing atmospheres (i.e., O-SMSI),[31] let alone that in non-oxide systems. For example, Au NPs supported on ZnO nanorods[31] and hydroxyapatite[23] could form SMSI states in O_2 atmosphere. Dong et al.[20] reported the classical SMSI effect between Ni and h-BN in weak oxidative atmospheres such as H_2O and CO_2. However, a deep insight into the O-SMSI process in metal/h-BN systems remains less explored, particularly for its comparison with classical SMSI processes.

In this work, we report the O-SMSI effect between Pt NPs and inert h-BN under oxidative conditions, in which Pt NPs are encapsulated by BO_x overlayers derived from the h-BN support. Over-encapsulation suppresses the surface adsorption of gas molecules and results in lower catalytic performance of Pt NPs in the CO oxidation reaction (COOX). Interestingly, precise manipulation of the SMSI state could be achieved by a facile washing process in hot water (90 °C) to de-encapsulate the Pt NPs, and residual trace amounts of BO_x overlayers can work synergistically with adjacent surface Pt sites, enhancing COOX activity significantly. The O-SMSI effect has been

Received: March 23, 2021
Accepted: April 19, 2021

https://doi.org/10.1021/acs.jpclett.1c00934
J. Phys. Chem. Lett. 2021, 12, 4187–4194

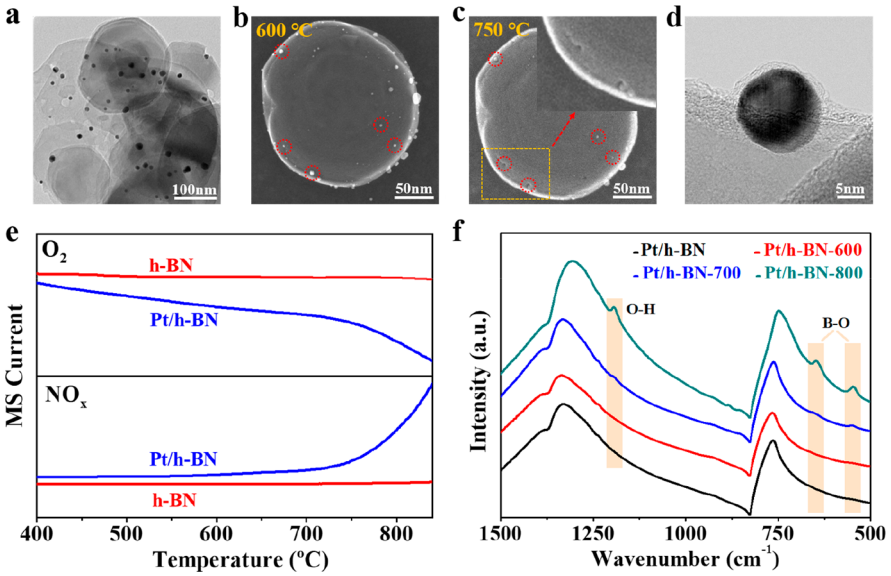

Figure 1. (a) TEM image of Pt/h-BN-800. (b, c) ESTEM images in the SE mode showing *in situ* evolution of an as-prepared Pt/h-BN sample in ~4 Pa O_2 atmosphere at the indicated temperatures. The inset shows the embedding of Pt NPs. (d) HRTEM image of a typical Pt NP in Pt/h-BN-800. (e) Mass spectroscopy (MS) signals of O_2-TPRe experiments over h-BN and Pt/h-BN. NO_x represents the mixture of NO and NO_2. (f) FT-IR spectra of Pt/h-BN, Pt/h-BN-600, Pt/h-BN-700, and Pt/h-BN-800.

successfully extended to other h-BN-supported noble metal catalysts. It has been revealed that the occurrence of the O-SMSI in metal/h-BN systems mainly depends on the metal−boron interaction and the O affinity of metals; the activation of oxidative gaseous molecules on the metal surface, such as O_2 and CO_2, also plays a critical role.

h-BN-supported Pt NPs (Pt/h-BN) were prepared by an impregnation method (see details in the Supporting Information) and then calcined at 600, 700, and 800 °C in air; these are denoted as Pt/h-BN-600, Pt/h-BN-700, and Pt/h-BN-800, respectively. X-ray diffraction (XRD) patterns and transmission electron microscopy (TEM) images of Pt/h-BN and Pt/h-BN-T (T = 600, 700, and 800 °C) are shown in Figures S1 and S2, and it is seen that the particle size of Pt NPs increases with the calcination temperature. Further, some obvious holes surrounding Pt NPs on h-BN sheets are observed in Pt/h-BN-800 (Figure 1a) but not in the other Pt/h-BN (Figure S2) and pure h-BN-800 (Figure S3) samples, which indicates the Pt-aided etching of h-BN at elevated temperatures.

Environmental scanning transmission electron microscopy (ESTEM) was used to *in situ* track the etching of an as-prepared Pt/h-BN at elevated temperatures in an O_2 atmosphere (~4 Pa). Along with high-angle annular dark-field (HAADF) and bright-field (BF) images, secondary electron (SE) images were acquired to enhance the surface sensitivity. As shown in Figures S4a,b and 1b, at low temperatures (200−600 °C) the surface of h-BN nanosheets is relatively smooth, and Pt particles all remain on the top of the h-BN surface. When the temperature is increased to 700 °C, nanopits close to Pt NPs appear at the Pt/h-BN interface (Figure S4c,d), and some small Pt NPs are even embedded into the h-BN at 750 °C (Figure 1c). Therefore, both *ex situ* and *in situ* TEM images confirm the etching of h-BN at the interfacial sites between Pt and h-BN at elevated temperatures. A high-resolution transmission electron microscopy (HRTEM) image of Pt/h-BN-800 is shown in Figures 1d and S5, indicating that Pt NPs are covered by amorphous overlayers. In contrast, Pt NPs in the fresh Pt/h-BN sample (Figure S6) have bare surfaces. Energy-dispersive spectroscopy (EDS) elemental mapping analysis (Figure S7) was further conducted, and its turns out that the amorphous overlayers consist of B and O elements. Thus, we conclude that Pt NPs are encapsulated by amorphous BO_x overlayers, which happens during the etching of h-BN sheets.

O_2 temperature-programmed reaction (O_2-TPRe) experiments have been performed over Pt/h-BN and pure h-BN under 5% O_2 /Ar atmospheres, as shown in Figure 1e. A rapid increase of gaseous nitrogen oxide compounds (NO_x, mixture of NO and NO_2, m/z = 30) has been observed above 600 °C for Pt/h-BN, while no obvious NO_x signal appears for the pure h-BN below 800 °C. The results suggest that the etching reactions between O_2 and h-BN strongly depend on the presence of Pt NPs. Fourier transform infrared spectroscopy (FT-IR) results in Figure 1f show three groups of new bands in Pt/h-BN-700 compared with Pt/h-BN and Pt/h-BN-600, in which the group of peaks located at 540−750 cm^{-1} originates from O−B−O bonds and the peak around 1196 cm^{-1} originates from O−H.[13] In addition, the intensity of B−O bonding increases with the oxidation temperature, which indicates the formation of BO_x species above 700 °C, consistent with the ESTEM and O_2-TPRe experiments. The above results suggest that the Pt-aided oxidative etching of h-BN generates surface BO_x and gaseous NO_x (NO and NO_2) species, which can be described by the equation $O_2(g)$ + $BN(s) \rightarrow BO_x(s) + NO_y(g)$.

Encapsulation of metal NPs with support-derived material overlayers is a typical characteristic of the classical SMSI effect in oxide-supported metal catalysts.[21,22,32] Here, we have demonstrated the presence of the O-SMSI effect between Pt NPs and h-BN support upon high-temperature oxidation treatment. Another typical feature of the SMSI effect is that encapsulation and de-encapsulation are reversible under alternative oxidation and reduction conditions.[29,33] It has been known that encapsulation usually leads to the suppression of surface adsorption of small molecules such as CO and H_2,

https://doi.org/10.1021/acs.jpclett.1c00934
J. Phys. Chem. Lett. 2021, 12, 4187−4194

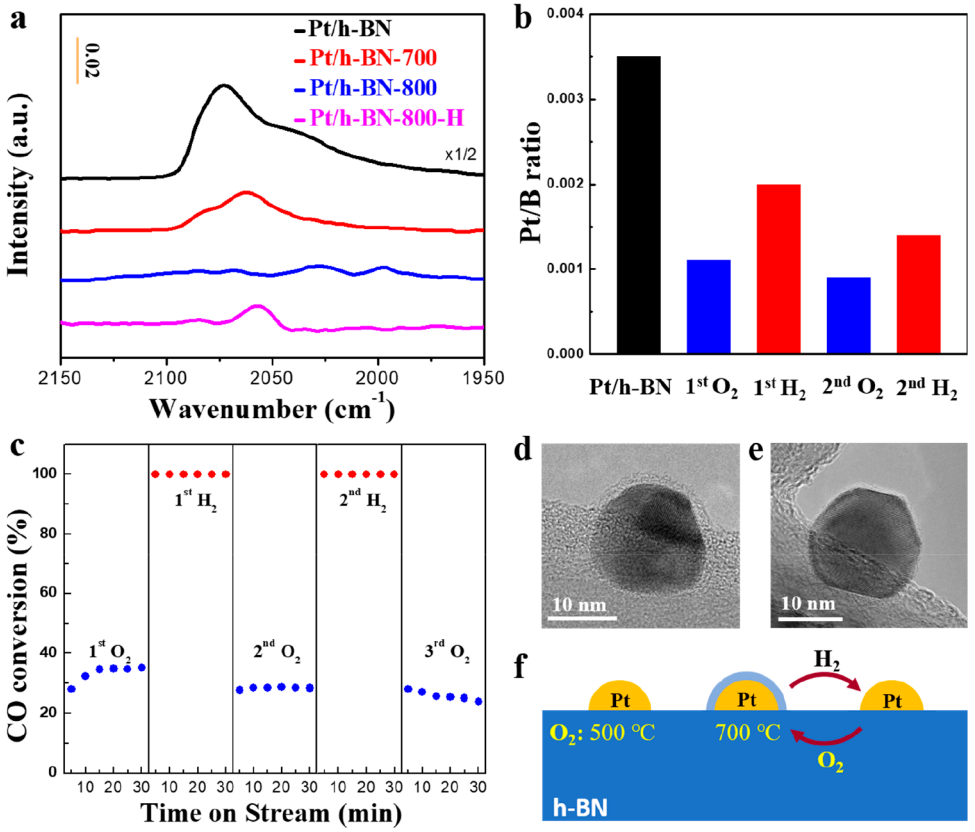

Figure 2. (a) DRIFTS spectra of CO adsorption on Pt/h-BN, Pt/h-BN-700, Pt/h-BN-800, and Pt/h-BN-800-H. (b) Pt/B atomic ratio of Pt/h-BN subjected to alternative treatments in O_2 at 700 °C for 4 h and in H_2 at 800 °C for 2 h as derived from XPS analysis (Figure S8). (c) CO conversions with time-on-stream at 183 °C over the Pt/h-BN sample subjected to alternative treatments in air at 700 °C and in H_2 at 800 °C. Gas flow: 1% CO, 20% O_2, 1% N_2, and balanced with He, space velocity (SV) = 20 000 mL·g_{cat}^{-1}·h^{-1}. HRTEM images of (d) Pt/h-BN-700 and (e) Pt/h-BN-700-H. (f) Schematic diagram of the O-SMSI effect in Pt/h-BN catalyst, showing the reversible structure evolution of Pt NPs.

which can be well confirmed by the surface adsorption experiments.[27] Therefore, diffuse reflectance infrared Fourier transform spectroscopic (DRIFTS) experiments of CO adsorption were performed to investigate the reversibility of the SMSI state. Figure 2a shows that the strong CO adsorption band can be detected over the fresh Pt/h-BN. Only a very weak CO signal appears with Pt/h-BN-700, and no CO adsorption band is detected on Pt/h-BN-800, suggesting that the Pt NPs are almost completely covered by BO_x overlayers. In contrast, the CO adsorption band presents an increase in peak intensity after H_2 treatment at 800 °C for 2 h (denoted as Pt/h-BN-800-H). The re-appearance of the CO adsorption band can be attributed to the recovery of the exposed Pt surface.

X-ray photoelectron spectroscopy (XPS) and FT-IR were further applied to characterize the surface composition of various Pt/h-BN samples. The Pt/B atomic ratio (Figures 2b and S8) determined by XPS decreases from 0.0035 in fresh Pt/h-BN to 0.0011 in Pt/h-BN-700, while BO_x species appear (Figures S9) in Pt/h-BN-700, which is consistent with the encapsulation of Pt NPs by BO_x overlayers. When Pt/h-BN-700 is treated in H_2 at 800 °C, the Pt/B atomic ratio increases to 0.0020 and BO_x species disappear, indicating that surface BO_x overlayers are removed under H_2 treatment.[34] With the second cyclic treatment in O_2 and H_2 atmospheres, the mean size of Pt NPs has no change (14−15 nm, seen in Figure S10), while the Pt/B atomic ratio decreases and increases, respectively, which confirms the reversible structural transformation between the BO_x-covered Pt NPs and bare Pt NPs under the cycled oxidation and reduction treatments.

In the classical SMSI state, active metal surface sites are covered by surface overlayers, which often suppress catalytic reactions.[28,35] Here, COOX was tested over the Pt/h-BN catalysts subjected to alternative O_2 and H_2 treatments. As shown in Figure 2c, after treatment in air at 700 °C, the COOX activity is always lower than that after treatment in H_2 at 800 °C. The COOX performance change can be assigned to the encapsulation of Pt NPs under O_2 treatment and re-exposure of the Pt NPs surface under H_2 treatment. HRTEM images (Figures 2d,e and S11) verify that the amorphous overlayers disappear after H_2 treatment of Pt/h-BN-700 at 800 °C as well. Overall, the O-SMSI effect in Pt/h-BN is illustrated by Figure 2f, which is very similar to the classical SMSI effect in metal/oxide systems except that the encapsulation and de-encapsulation are reversible under cycled oxidation and reduction treatments in metal/h-BN systems but under cycled reduction and oxidation treatments for the metal/oxide systems.

Since the SMSI state involving the encapsulation of Pt NPs by BO_x would deactivate the catalysts due to covering of the surface sites, it is important to properly modulate the SMSI state in order to obtain high activity of Pt/h-BN catalysts. For instance, Cao et al.[36] obtained atomically dispersed FeO_x species on Pt NPs by accurately controlling the amount of deposited FeO_x using atomic layer deposition, maximizing active Pt-FeO_x interfacial sites. Herein, the knowledge that

https://doi.org/10.1021/acs.jpclett.1c00934
J. Phys. Chem. Lett. 2021, 12, 4187−4194

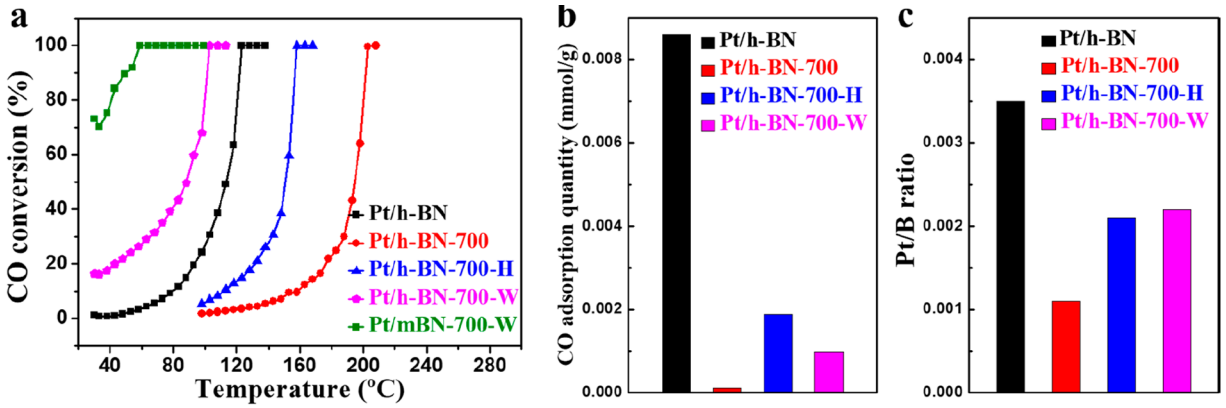

Figure 3. (a) COOX light-off curves of Pt/h-BN, Pt/h-BN-700, Pt/h-BN-700-H, Pt/h-BN-700-W, and Pt/mBN-700-W catalysts. Gas flow: 1% CO, 20% O_2, 1% N_2, and balanced with He, SV = 20 000 $mL \cdot g_{cat}^{-1} \cdot h^{-1}$. (b) CO adsorption amount on Pt/h-BN-700, Pt/h-BN-700-H, and Pt/h-BN-700-W at 50 °C, based on CO pulse chemisorption experiments. (c) Pt/B atomic ratio of Pt/h-BN, Pt/h-BN-700, Pt/h-BN-700-H, and Pt/h-BN-700-W derived from XPS spectra (Figure S12).

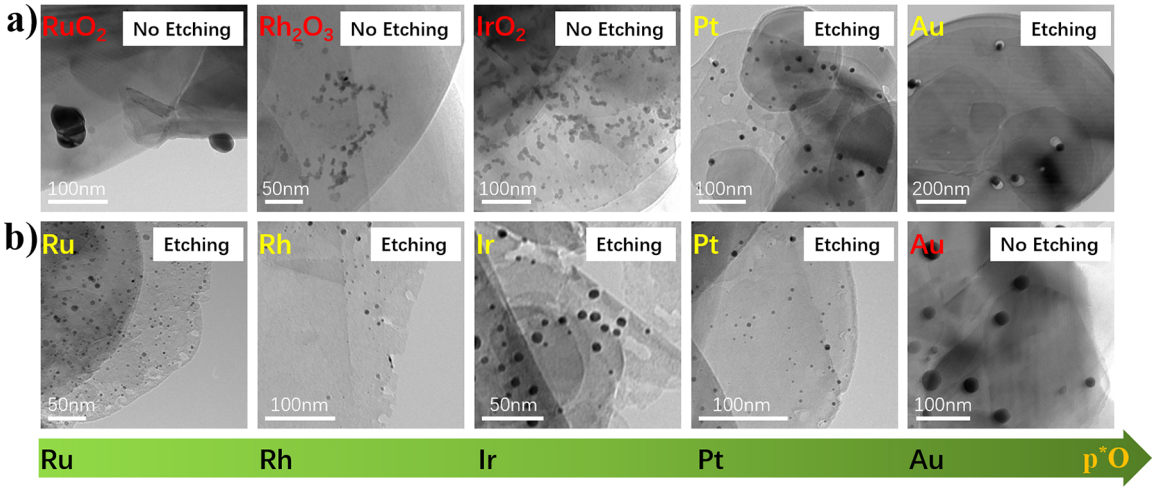

Figure 4. TEM images of noble metal (NM)/h-BN samples (NM = Ru, Rh, Ir, Pt, and Au) treated at 800 °C in (a) O_2 and (b) CO_2 atmosphere. Oxygen affinity (p*O) of the NMs decreases from left to right.[41]

boron oxides can be dissolved in hot water could be used to remove the BO_x overlayers covering the Pt NPs surface. So, Pt/h-BN-700 was subjected to washing in hot water (90 °C), and the resulting samples are denoted as Pt/h-BN-700-W.

Pt/h-BN-700-W shows COOX activity with a T_{100} of 100 °C, which is better than that of the fresh Pt/h-BN and Pt/h-BN-700-H catalysts (Figure 3a). CO pulse chemisorption experiments (Figure 3b) indicate that the CO adsorption quantity of Pt/h-BN-700-W is higher than that of Pt/h-BN-700. XPS results in Figure 3c prove higher surface Pt/B atomic ratio for Pt/h-BN-700-W compared with Pt/h-BN-700. Together with the reduction of BO_x species shown in FT-IR spectra (Figure S13), all this evidence demonstrates that significant surface BO_x species are removed after the water-washing and part of Pt NPs surfaces are re-exposed. The HRTEM image and EDS mapping data (Figure S14) also reveal that there are fewer amorphous BO_x overlayers remaining on the surface of Pt NPs after the washing treatments. Accordingly, we speculate that there exist Pt−O−B chemical bonds at the Pt−BO_x interfaces and BO_x overlayers cannot be fully dissolved during the washing treatment, leaving partially re-exposed Pt surfaces. The better COOX performance of Pt/h-BN-700-W is attributed to the newly formed interfaces between residual BO_x overlayers and neighboring Pt surface sites, which have been well proved to act as the active centers to dissociate O_2 in many oxide/metal inverse catalysts.[36−38] Compared with H_2 treatment at high temperatures, the facile water-washing treatment not only removes the excess BO_x overlayers on Pt NPs but also creates new Pt-BO_x interfacial sites, which lead to promoted COOX activity compared to bare Pt NPs.

To maximize Pt-BO_x interfacial active sites, a ball-milling method[39] was used to prepare BN (denoted as mBN) with high specific surface area (~101 m^2/g, determined by BET analysis). Pt/mBN-700-W was prepared by the same method as Pt/h-BN-700-W except that mBN was used as the support. As shown in Figure 3a, Pt/mBN-700-W shows extraordinary COOX activity with a T_{100} of 60 °C, in contrast with T_{100} at 100 °C for Pt/h-BN-700-W; Pt/mBN-700-W also displays the lowest activation energy (E_a) of 19.5 kJ/mol among all the samples (Figure S15), close to the E_a reported in Pt/Fe(OH)$_x$ catalysts (16 kJ/mol).[40] TEM images in Figure S16 indicate that Pt/mBN-700-W presents a smaller size distribution of Pt NPs than Pt/h-BN-700-W. Thus, a high density of Pt-BO_x interfacial sites in Pt/mBN-700-W is expected, which results in the enhanced COOX activity.

https://doi.org/10.1021/acs.jpclett.1c00934
J. Phys. Chem. Lett. 2021, 12, 4187−4194

So far, the O-SMSI effect between Pt NPs and h-BN and its influence on catalysis have been well demonstrated. Besides Pt, the O-SMSI effect has been systematically investigated in other h-BN-supported noble metals (NMs). Here, oxidative etching of h-BN with NM/h-BN (NM = Ru, Rh, Ir, Pt, and Au) systems was discussed first at an O_2 atmosphere. All the NM/h-BN samples were treated in air at 800 °C (denoted as metal/h-BN-800). TEM images (Figure 4a) show that oxidative etching of h-BN in an O_2 atmosphere only happens with Au/h-BN-800, which shows behavior similar to that of Pt/h-BN-800. O_2-TPRe experiments have been performed over all the NM/h-BN samples at 5% O_2/Ar atmosphere (Figures 1d and S17). The consumption of O_2 and formation of NO_x have been observed above 600 °C in Pt/h-BN and Au/h-BN, which suggests the same etching reactions between O_2 and h-BN. In contrast, there is much less consumption of O_2 over the other NM/h-BN systems (NM = Ru, Rh, and Ir). XRD patterns (Figures S18−S22) indicate that RuO_2, Rh_2O_3, and IrO_2 formed in the NM/h-BN-800 samples (NM = Ru, Rh, and Ir), while the supported Pt and Au NPs stay in the metallic state after O_2 treatment at 800 °C. These results indicate that it is necessary to keep the metallic state of NMs under the high-temperature oxidation conditions in order to trigger the oxidative etching of h-BN. Accordingly, we infer that O_2 can be activated on metallic Pt and Au but not on the oxides of Rh_2O_3, IrO_2, and RuO_2 to produce dissociative atomic O species, which then diffuse to the NM/h-BN interfaces and oxidize the h-BN sheets.

Another oxidative atmosphere (5% CO_2/Ar) was used to verify the triggering mechanism of the O-SMSI effect in the NM/h-BN systems. All NM/h-BN samples (NM = Pt, Au, Ru, Rh, and Ir) were treated in 5% CO_2/Ar at 800 °C. XRD results show that all the metals stay in the metallic state after high-temperature treatment in CO_2 (Figures S18−S22). However, the oxidative etching of h-BN was only observed for Pt, Ru, Rh, and Ir, while the h-BN sheets show no obvious change in Au/h-BN (Figure 4b). CO_2-TPRe experiments have been performed over all the NM/h-BN samples under 5% CO_2/Ar atmosphere. As shown in Figures S23−S27, consumption of CO_2 and significant formation of CO, N_2, and NO_x appear around 700 °C, except for the Au/h-BN, suggesting that CO_2 is dissociated on the NM/h-BN (NM = Pt, Ru, Rh, and Ir) samples but not on Au/h-BN at 800 °C. In our previous work,[20] the metal-aided etching of h-BN in CO_2 was also observed in non-noble transition metals (Fe, Co, and Ni) when supported on h-BN. The distinct behavior of Au may be ascribed to the lower dissociative adsorption tendency of CO_2 on Au than on the other metals' surfaces. The dissociation of CO_2 into CO and O species and subsequent spillover of O atoms to the metal/h-BN interfaces help to oxidize the h-BN sheets.[42] The present experiments demonstrate that the activation of CO_2 occurs on Pt, Ru, Rh, Ir, Fe, Co, and Ni but not on Au at the high temperature.[43,44]

The experimental results of the oxidative etching of h-BN in transition metal (TM)/h-BN systems under O_2 and CO_2 atmospheres are summarized in Figure 5. Corresponding values of the enthalpy of formation of TM-B alloy and O affinity (p*O) of various metals are also presented. Based on all this work and reported results, available atmospheric conditions for the oxidative etching of h-BN in TM/h-BN systems are as follows: O_2 for Pt/h-BN, Au/h-BN, and Ag/h-BN;[47] CO_2 for TM/h-BN (TM = Pt, Ru, Rh, Ir, Ni, Fe, and Co).[20] It has been proven that the interface stability of metal−

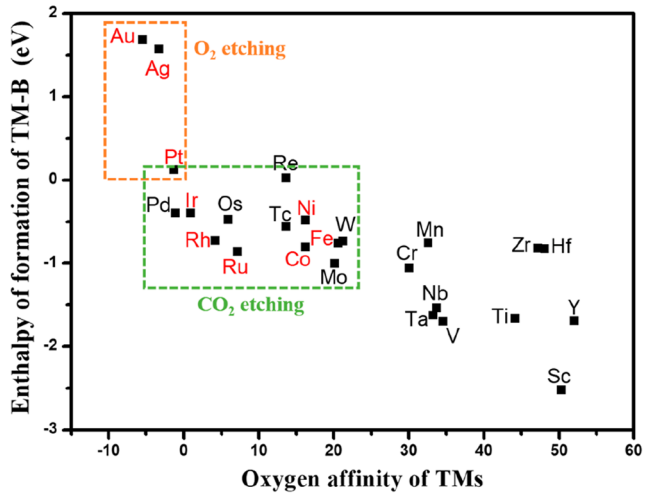

Figure 5. Correlation between metal-aided oxidative etching of h-BN in various TM/h-BN systems under two atmospheres and the enthalpy of formation of TM-B binary compounds[45,46] and the p*O of metals.[41] Metals highlighted by red color have shown the etching phenomena under corresponding atmospheres either in this work or reported works.

carbon or metal−boron plays an important role in the etching reaction of graphene or h-BN.[48−50] For example, the Ni−carbon interaction acted as the driving force to cut graphene.[49] Here, we show that, at O_2 atmosphere, low p*O of TM and weak TM−boron binding energy (Au, Pt, and Ag) seem to be the prerequisite conditions toward successful etching of the h-BN sheets. The low p*O of metal is conducive to maintain its metallic state in the O_2 atmosphere and at the high temperature, and the oxidative ability of oxygen is strong enough to break the B−N bonds, even with little assistance of the TM−boron interaction. In CO_2 atmosphere, although TMs (Ir, Rh, Ru, Fe, Co, and Ni) can keep their metallic state, the weak oxidative ability of CO_2 demands stronger TM−boron binding energy to assist the breakage of B−N bonds. Therefore, the etching behaviors in Figure 5 could be understood based on the formation enthalpy of TM-B alloy and the p*O of metals. It should also be noted that the activation of gaseous molecules (O_2 and CO_2) on the metal surface plays a critical role. Under the reaction conditions, i.e., ambient pressure and 800 °C, O_2 can be activated on metallic Pt and Au but not on oxides, such like RuO_x, RhO_x, and IrO_x, while CO_2 can be activated on Ru, Rh, Pt, and Ir but not on Au.[44]

In summary, we demonstrate the O-SMSI effect on the Pt/h-BN system, in which Pt-aided oxidative etching of h-BN sheets close to Pt NPs has been induced in O_2 atmospheres at elevated temperatures and the amorphous BO_x species simultaneously migrate onto Pt NPs to form BO_x encapsulation overlayers. A water-washing method is proved to be facile and effective to manipulate the O-SMSI state, and the residual BO_x species work synergistically with adjacent Pt surface sites to enhance the COOX activity significantly. Moreover, the O-SMSI effect observed between Pt and inert h-BN support has been extended to other h-BN-supported metal catalysts, and the critical factors to trigger the O-SMSI effect have been concluded. Our results not only enrich the understanding of the SMSI concept but also provide practical guidance in the design and application of h-BN-supported metal catalysts.

https://doi.org/10.1021/acs.jpclett.1c00934
J. Phys. Chem. Lett. 2021, 12, 4187−4194

■ ASSOCIATED CONTENT

Supporting Information

The Supporting Information is available free of charge at https://pubs.acs.org/doi/10.1021/acs.jpclett.1c00934.

Experimental procedures and characterization data for various samples, including Figures S1−S27 (PDF)

■ AUTHOR INFORMATION

Corresponding Author

Qiang Fu − *State Key Laboratory of Catalysis, iChEM, Dalian Institute of Chemical Physics, Chinese Academy of Science, Dalian 116023, China; Dalian National Laboratory for Clean Energy, Dalian Institute of Chemical Physics, Chinese Academy of Sciences, Dalian 116023, China;* orcid.org/0000-0001-5316-6758; Email: qfu@dicp.ac.cn

Authors

Tongyuan Song − *State Key Laboratory of Catalysis, iChEM, Dalian Institute of Chemical Physics, Chinese Academy of Science, Dalian 116023, China; University of Chinese Academy of Sciences, Beijing 100049, China*

Jinhu Dong − *State Key Laboratory of Catalysis, iChEM, Dalian Institute of Chemical Physics, Chinese Academy of Science, Dalian 116023, China*

Rongtan Li − *State Key Laboratory of Catalysis, iChEM, Dalian Institute of Chemical Physics, Chinese Academy of Science, Dalian 116023, China; University of Chinese Academy of Sciences, Beijing 100049, China;* orcid.org/0000-0003-2061-3368

Xiaoyan Xu − *Dalian National Laboratory for Clean Energy, Dalian Institute of Chemical Physics and CAS Key Laboratory of Science and Technology on Applied Catalysis, Dalian Institute of Chemical Physics, Chinese Academy of Sciences, Dalian 116023, China*

Matsumoto Hiroaki − *Hitachi High-Tech (Shanghai) Co., Ltd., Shanghai 201203, P. R. China*

Bing Yang − *Dalian National Laboratory for Clean Energy, Dalian Institute of Chemical Physics and CAS Key Laboratory of Science and Technology on Applied Catalysis, Dalian Institute of Chemical Physics, Chinese Academy of Sciences, Dalian 116023, China;* orcid.org/0000-0003-3515-0642

Rankun Zhang − *State Key Laboratory of Catalysis, iChEM, Dalian Institute of Chemical Physics, Chinese Academy of Science, Dalian 116023, China; Zhang Dayu School of Chemistry, Dalian University of Technology, Dalian 116024, China*

Yunxing Bai − *State Key Laboratory of Catalysis, iChEM, Dalian Institute of Chemical Physics, Chinese Academy of Science, Dalian 116023, China; Dalian National Laboratory for Clean Energy, Dalian Institute of Chemical Physics, Chinese Academy of Sciences, Dalian 116023, China*

Hui Xin − *State Key Laboratory of Catalysis, iChEM, Dalian Institute of Chemical Physics, Chinese Academy of Science, Dalian 116023, China; Dalian National Laboratory for Clean Energy, Dalian Institute of Chemical Physics, Chinese Academy of Sciences, Dalian 116023, China*

Le Lin − *State Key Laboratory of Catalysis, iChEM, Dalian Institute of Chemical Physics, Chinese Academy of Science, Dalian 116023, China*

Rentao Mu − *State Key Laboratory of Catalysis, iChEM, Dalian Institute of Chemical Physics, Chinese Academy of Science, Dalian 116023, China; Dalian National Laboratory for Clean Energy, Dalian Institute of Chemical Physics, Chinese Academy of Sciences, Dalian 116023, China*

Xinhe Bao − *State Key Laboratory of Catalysis, iChEM, Dalian Institute of Chemical Physics, Chinese Academy of Science, Dalian 116023, China; Dalian National Laboratory for Clean Energy, Dalian Institute of Chemical Physics, Chinese Academy of Sciences, Dalian 116023, China;* orcid.org/0000-0001-9404-6429

Complete contact information is available at: https://pubs.acs.org/10.1021/acs.jpclett.1c00934

Author Contributions

#T.S. and J.D. contributed equally to this work.

Notes

The authors declare no competing financial interest.

■ ACKNOWLEDGMENTS

This work was financially supported by the National Natural Science Foundation of China (No. 21825203, No. 21688102, and No. 91945302), the Ministry of Science and Technology of China (No. 2016YFA0200200 and No. 2017YFB0602205), the Strategic Priority Research Program of the Chinese Academy of Sciences (Grant No. XDB17020000), and the Dalian National Laboratory for Clean Energy (DNL) Cooperation Fund (DNL201907).

■ REFERENCES

(1) Grant, J. T.; Carrero, C. A.; Goeltl, F.; Venegas, J.; Mueller, P.; Burt, S. P.; Specht, S. E.; McDermott, W. P.; Chieregato, A.; Hermans, I. Selective oxidative dehydrogenation of propane to propene using boron nitride catalysts. *Science* **2016**, *354* (6319), 1570−1573.

(2) Shi, L.; Wang, D.; Song, W.; Shao, D.; Zhang, W.; Lu, A. Edge-hydroxylated boron nitride for oxidative dehydrogenation of propane to propylene. *ChemCatChem* **2017**, *9* (10), 1788−1793.

(3) Liu, Z.; Liu, J.; Mateti, S.; Zhang, C.; Zhang, Y.; Chen, L.; Wang, J.; Wang, H.; Doeven, E. H.; Francis, P. S.; Barrow, C. J.; Du, A.; Chen, Y.; Yang, W. Boron radicals identified as the source of the unexpected catalysis by boron nitride nanosheets. *ACS Nano* **2019**, *13* (2), 1394−1402.

(4) Shtansky, D. V.; Firestein, K. L.; Golberg, D. V. Fabrication and application of BN nanoparticles, nanosheets and their nanohybrids. *Nanoscale* **2018**, *10* (37), 17477−17493.

(5) Wang, Y.; Zhao, L.; Shi, L.; Sheng, J.; Zhang, W.; Cao, X.; Hu, P.; Lu, A. Methane activation over a boron nitride catalyst driven by in situ formed molecular water. *Catal. Sci. Technol.* **2018**, *8* (8), 2051−2055.

(6) Hu, Y.; Zheng, W.; Jia, A.; Luo, M.; Tang, C.; Lu, J. Selective hydrogenation of crotonaldehyde over Ir/BN catalysts: kinetic investigation and Ir particle size effect. *React. Kinet., Mech. Catal.* **2021**, *132*, 301−305.

(7) Pakdel, A.; Bando, Y.; Golberg, D. Nano boron nitride flatland. *Chem. Soc. Rev.* **2014**, *43* (3), 934−959.

(8) Huang, R.; Zhang, B.; Wang, J.; Wu, K.; Shi, W.; Zhang, Y.; Liu, Y.; Zheng, A.; Schlögl, R.; Su, D. Direct insight into ethane oxidative dehydrogenation over boron nitrides. *ChemCatChem* **2017**, *9* (17), 3293−3297.

(9) Shi, L.; Wang, D.; Lu, A. A viewpoint on catalytic origin of boron nitride in oxidative dehydrogenation of light alkanes. *Chin. J. Catal.* **2018**, *39* (5), 908−913.

(10) Love, A. M.; Thomas, B.; Specht, S. E.; Hanrahan, M. P.; Venegas, J. M.; Burt, S. P.; Grant, J. T.; Cendejas, M. C.; McDermott, W. P.; Rossini, A. J.; Hermans, I. Probing the transformation of boron

nitride catalysts under oxidative dehydrogenation conditions. *J. Am. Chem. Soc.* **2019**, *141* (1), 182−190.
(11) Zhou, Y.; Lin, J.; Li, L.; Pan, X.; Sun, X.; Wang, X. Enhanced performance of boron nitride catalysts with induction period for the oxidative dehydrogenation of ethane to ethylene. *J. Catal.* **2018**, *365*, 14−23.
(12) Zhu, W.; Wu, Z.; Foo, G. S.; Gao, X.; Zhou, M.; Liu, B.; Veith, G. M.; Wu, P.; Browning, K. L.; Lee, H. N.; Li, H.; Dai, S.; Zhu, H. Taming interfacial electronic properties of platinum nanoparticles on vacancy-abundant boron nitride nanosheets for enhanced catalysis. *Nat. Commun.* **2017**, *8* (1), 15291.
(13) Konopatsky, A. S.; Firestein, K. L.; Leybo, D. V.; Popov, Z. I.; Larionov, K. V.; Steinman, A. E.; Kovalskii, A. M.; Matveev, A. T.; Manakhov, A. M.; Sorokin, P. B.; Golberg, D.; Shtansky, D. V. BN nanoparticle/Ag hybrids with enhanced catalytic activity: theory and experiments. *Catal. Sci. Technol.* **2018**, *8* (6), 1652−1662.
(14) Fan, M.; Jimenez, J. D.; Shirodkar, S. N.; Wu, J.; Chen, S.; Song, L.; Royko, M. M.; Zhang, J.; Guo, H.; Cui, J.; Zuo, K.; Wang, W.; Zhang, C.; Yuan, F.; Vajtai, R.; Qian, J.; Yang, J.; Yakobson, B. I.; Tour, J. M.; Lauterbach, J.; Sun, D.; Ajayan, P. M. Atomic Ru Immobilized on Porous h-BN through Simple Vacuum Filtration for Highly Active and Selective CO_2 Methanation. *ACS Catal.* **2019**, *9* (11), 10077−10086.
(15) Zhao, H.; Song, J.; Song, X.; Yan, Z.; Zeng, H. Ag/white graphene foam for catalytic oxidation of methanol with high efficiency and stability. *J. Mater. Chem. A* **2015**, *3* (12), 6679−6684.
(16) Bu, K.; Kuboon, S.; Deng, J.; Li, H.; Yan, T.; Chen, G.; Shi, L.; Zhang, D. Methane dry reforming over boron nitride interface-confined and LDHs-derived Ni catalysts. *Appl. Catal., B* **2019**, *252*, 86−97.
(17) Bu, K.; Deng, J.; Zhang, X.; Kuboon, S.; Yan, T.; Li, H.; Shi, L.; Zhang, D. Promotional effects of B-terminated defective edges of Ni/boron nitride catalysts for coking-and sintering-resistant dry reforming of methane. *Appl. Catal., B* **2020**, *267*, 118692.
(18) Cao, Y.; Maitarad, P.; Gao, M.; Taketsugu, T.; Li, H.; Yan, T.; Shi, L.; Zhang, D. Defect-induced efficient dry reforming of methane over two-dimensional Ni/h-boron nitride nanosheet catalysts. *Appl. Catal., B* **2018**, *238*, 51−60.
(19) Liu, Y.; Li, X.; Liao, W.; Jia, A.; Wang, Y.; Luo, M.; Lu, J. Highly Active Pt/BN Catalysts for Propane Combustion: The Roles of Support and Reactant-Induced Evolution of Active Sites. *ACS Catal.* **2019**, *9* (2), 1472−1481.
(20) Dong, J.; Fu, Q.; Li, H.; Xiao, J.; Yang, B.; Zhang, B.; Bai, Y.; Song, T.; Zhang, R.; Gao, L.; Cai, J.; Zhang, H.; Liu, Z.; Bao, X. Reaction-Induced Strong Metal−Support Interactions between Metals and Inert Boron Nitride Nanosheets. *J. Am. Chem. Soc.* **2020**, *142* (40), 17167−17174.
(21) Liu, J. Advanced electron microscopy of metal−support interactions in supported metal catalysts. *ChemCatChem* **2011**, *3* (6), 934−948.
(22) Kuwauchi, Y.; Yoshida, H.; Akita, T.; Haruta, M.; Takeda, S. Intrinsic catalytic structure of gold nanoparticles supported on TiO_2. *Angew. Chem., Int. Ed.* **2012**, *51* (31), 7729−7733.
(23) Tang, H.; Wei, J.; Liu, F.; Qiao, B.; Pan, X.; Li, L.; Liu, J.; Wang, J.; Zhang, T. Strong Metal-Support Interactions between Gold Nanoparticles and Nonoxides. *J. Am. Chem. Soc.* **2016**, *138* (1), 56−59.
(24) Tang, H.; Liu, F.; Wei, J.; Qiao, B.; Zhao, K.; Su, Y.; Jin, C.; Li, L.; Liu, J.; Wang, J.; Zhang, T. Ultrastable Hydroxyapatite/Titanium-Dioxide-Supported Gold Nanocatalyst with Strong Metal-Support Interaction for Carbon Monoxide Oxidation. *Angew. Chem.* **2016**, *128* (36), 10764−10769.
(25) van Deelen, T. W.; Hernández Mejía, C.; de Jong, K. P. Control of metal-support interactions in heterogeneous catalysts to enhance activity and selectivity. *Nat. Catal.* **2019**, *2* (11), 955−970.
(26) Wang, L.; Zhang, J.; Zhu, Y.; Xu, S.; Wang, C.; Bian, C.; Meng, X.; Xiao, F. Strong Metal−Support Interactions Achieved by Hydroxide-to-Oxide Support Transformation for Preparation of Sinter-Resistant Gold Nanoparticle Catalysts. *ACS Catal.* **2017**, *7* (11), 7461−7465.
(27) Tauster, S. J.; Fung, S. C.; Garten, R. L. Strong Metal-Support Interactions. Group 8 Noble Metals Supported on $Ti0_2$. *J. Am. Chem. Soc.* **1978**, *100* (1), 170−175.
(28) Willinger, M. G.; Zhang, W.; Bondarchuk, O.; Shaikhutdinov, S.; Freund, H. J.; Schlogl, R. A case of strong metal-support interactions: combining advanced microscopy and model systems to elucidate the atomic structure of interfaces. *Angew. Chem., Int. Ed.* **2014**, *53* (23), 5998−6001.
(29) Anderson, J. B. F.; Burch, R.; Cairns, J. A. The Reversibility of the Strong Metal-Support Interaction under Reaction Conditions. *Appl. Catal.* **1986**, *21* (1), 179−185.
(30) Bernal, S.; Calvino, J. J.; Cauqui, M. A.; Gatica, J. M.; López Cartes, C.; Pérez Omil, J. A.; Pintado, J. M. Some contributions of electron microscopy to the characterisation of the strong metal−support interaction effect. *Catal. Today* **2003**, *77* (4), 385−406.
(31) Liu, X.; Liu, M.; Luo, Y.; Mou, C.; Lin, S.; Cheng, H.; Chen, J.; Lee, J. F.; Lin, T. Strong metal-support interactions between gold nanoparticles and ZnO nanorods in CO oxidation. *J. Am. Chem. Soc.* **2012**, *134* (24), 10251−10258.
(32) Ro, I.; Resasco, J.; Christopher, P. Approaches for Understanding and Controlling Interfacial Effects in Oxide-Supported Metal Catalysts. *ACS Catal.* **2018**, *8* (8), 7368−7387.
(33) Braunschweig, E. J.; Logan, A. D.; Daty, A. K.; Smith, D. J. Reversibility of Strong Metal-Support Interactions on $Rh/Ti0_2$. *J. Catal.* **1989**, *118* (1), 227−237.
(34) Sutter, P.; Lahiri, J.; Albrecht, P.; Sutter, E. Chemical vapor deposition and etching of high-quality monolayer hexagonal boron nitride films. *ACS Nano* **2011**, *5* (9), 7303−7309.
(35) Bonanni, S.; Aït-Mansour, K.; Brune, H.; Harbich, W. Overcoming the Strong Metal−Support Interaction State: CO Oxidation on TiO_2(110)-Supported Pt Nanoclusters. *ACS Catal.* **2011**, *1*, 385−389.
(36) Cao, L.; Liu, W.; Luo, Q.; Yin, R.; Wang, B.; Weissenrieder, J.; Soldemo, M.; Yan, H.; Lin, Y.; Sun, Z.; Ma, C.; Zhang, W.; Chen, S.; Wang, H.; Guan, Q.; Yao, T.; Wei, S.; Yang, J.; Lu, J. Atomically dispersed iron hydroxide anchored on Pt for preferential oxidation of CO in H_2. *Nature* **2019**, *565* (7741), 631−635.
(37) Fu, Q.; Li, W.; Yao, Y.; Liu, H.; Su, H.; Ma, D.; Gu, X.; Chen, L.; Wang, Z.; Zhang, H.; Wang, B.; Bao, X. Interface-confined ferrous centers for catalytic oxidation. *Science* **2010**, *328* (5982), 1141−1144.
(38) Ning, Y.; Wei, M.; Yu, L.; Yang, F.; Chang, R.; Liu, Z.; Fu, Q.; Bao, X. Nature of Interface Confinement Effect in Oxide/Metal Catalysts. *J. Phys. Chem. C* **2015**, *119* (49), 27556−27561.
(39) Lei, W.; Mochalin, V. N.; Liu, D.; Qin, S.; Gogotsi, Y.; Chen, Y. Boron nitride colloidal solutions, ultralight aerogels and freestanding membranes through one-step exfoliation and functionalization. *Nat. Commun.* **2015**, *6* (1), 8849.
(40) Chen, G.; Zhao, Y.; Fu, G.; Duchesne, P. N.; Gu, L.; Zheng, Y.; Weng, X.; Chen, M.; Zhang, P.; Pao, C. W.; Lee, J. F.; Zheng, N. Interfacial Effects in Iron-Nickel Hydroxide-Platinum Nanoparticles Enhance Catalytic Oxidation. *Science* **2014**, *344* (6183), 495−499.
(41) Reed, T. B. *Free Energy of Formation of Binary Compounds*; MIT Press: Cambridge, MA, 1971.
(42) Solymosi, F. The bonding, structure and reactions of CO_2 adsorbed on clean and promoted metal surfaces. *J. Mol. Catal.* **1991**, *65* (3), 337−358.
(43) Browne, V. M.; Carley, A. F.; Copperthwaite, R. G.; Davies, P. R.; Moser, E. M.; Roberts, M. W. Activation of carbon dioxide at bismuth, gold and copper surfaces. *Appl. Surf. Sci.* **1991**, *47* (4), 375−379.
(44) Freund, H. J.; Roberts, M. W. Surface chemistry of carbon dioxide. *Surf. Sci. Rep.* **1996**, *25* (8), 225−273.
(45) The Materials Project. Calculation of the enthalpy of formation of TM-B binary compounds using a database. https://materialsproject.org/#apps/reactioncalculator.
(46) Jain, A.; Hautier, G.; Ong, S. P.; Moore, C. J.; Fischer, C. C.; Persson, K. A.; Ceder, G. Formation enthalpies by mixing GGA and

https://doi.org/10.1021/acs.jpclett.1c00934
J. Phys. Chem. Lett. 2021, 12, 4187−4194

GGA+Ucalculations. *Phys. Rev. B: Condens. Matter Mater. Phys.* **2011**, *84* (4), 045115.
(47) Liao, Y.; Tu, K.; Han, X.; Hu, L.; Connell, J. W.; Chen, Z.; Lin, Y. Oxidative Etching of Hexagonal Boron Nitride Toward Nanosheets with Defined Edges and Holes. *Sci. Rep.* **2015**, *5* (1), 14510.
(48) Ma, L.; Wang, J.; Yip, J.; Ding, F. Mechanism of Transition-Metal Nanoparticle Catalytic Graphene. *J. Phys. Chem. Lett.* **2014**, *5* (7), 1192−1197.
(49) Qiu, Z.; Song, L.; Zhao, J.; Li, Z.; Yang, J. The Nanoparticle Size Effect in Graphene Cutting: A "Pac-Man" Mechanism. *Angew. Chem.* **2016**, *128* (34), 10072−10075.
(50) Ma, L.; Zeng, X. C. Catalytic Directional Cutting of Hexagonal Boron Nitride: The Roles of Interface and Etching Agents. *Nano Lett.* **2017**, *17* (5), 3208−3214.

https://doi.org/10.1021/acs.jpclett.1c00934
J. Phys. Chem. Lett. 2021, 12, 4187−4194